JOURNAL OF AIRCRAFT
Vol. 45, No. 4, July–August 2008

Thrust and Drag Models for Performance Calculations for High-Speed Aircraft

David H. Bridges*
Mississippi State University, Mississippi State, Mississippi 39762

DOI: 10.2514/1.34919

On the introductory level, aircraft performance analysis usually assumes that the thrust and the drag polar parameters are independent of Mach number. To perform analyses of high-speed aircraft, however, Mach number effects have to be included. This study describes models of thrust and drag that include Mach number effects and the application of these models to analyses of cruise speed, ceiling, and range, as well as to performance predictions that use energy methods.

Nomenclature

A_i	=	engine inlet area
a	=	speed of sound
C_{D0}	=	zero-lift drag coefficient
C_L	=	lift coefficient
C_p	=	specific heat at constant pressure
c	=	thrust-specific fuel consumption
E	=	lift-to-drag ratio
f	=	engine fuel-to-air ratio
f_{AB}	=	afterburner fuel-to-air ratio
h	=	altitude
k	=	induced-drag coefficient parameter in parabolic drag polar
M	=	Mach number
p	=	pressure
p_{ex}	=	specific excess power
p_0	=	stagnation pressure
pr	=	stagnation pressure ratio across engine component
R	=	gas constant
S	=	wing reference area
T	=	thrust, temperature
T_0	=	stagnation temperature
u, V	=	flight speed
W	=	weight
β	=	turbofan bypass ratio
γ	=	specific heat ratio
δ	=	ratio of ambient pressure to pressure at tropopause
ζ	=	cruise-fuel-weight fraction
ρ	=	density
ω	=	dimensionless wing-loading parameter

I. Introduction

THE basics of aircraft performance analysis are usually taught under the assumption that Mach number effects may be neglected. In particular, the aircraft thrust is usually assumed to be independent of aircraft speed (and therefore Mach number), as are the parameters C_{Do} and k in the parabolic drag polar:

$$C_D = C_{D0} + kC_L^2 \tag{1}$$

Although most textbooks do mention the effects of Mach number, particularly the rapid increase in C_{D0} around $M = 1$ known as the transonic drag rise, these effects are ignored to simplify the analysis and obtain results that are applicable to low-speed aircraft (see, for example, the textbooks by Hale [1] and Anderson [2]). Consequently, if these effects are ignored, it is possible to predict supersonic cruise velocities for aircraft such as the Boeing 767.

At least one textbook, a 1993 text by Vinh [3], deals with the analyses of high-performance aircraft in detail. In many of these analyses, Mach number effects are included. Vinh presents calculations of range, endurance, climbing flight, and turning flight that are all significantly impacted by the effects of Mach number. Another technique of predicting performance of high-speed aircraft that depends heavily upon correct inclusion of Mach number effects is the energy method, first described by Rutowski [4] and subsequently expanded upon by Bryson et al. [5], among others. To implement either the analyses of Vinh [3] or energy methods, it is necessary to have models of both thrust and drag as functions of Mach number and altitude. This paper will present models of each and will then illustrate their use in predictions of aircraft maximum speed, ceiling, and range, as well as in energy method analyses.

II. Thrust Model

The basic thrust model follows that of Hill and Peterson [6], which is obtained by breaking the standard aircraft turbojet or turbofan engine down into stages and performing a control volume analysis for each stage. The analysis that follows is for an augmented turbofan engine with an afterburner, such as the F100 engine in the F-15. An augmented turbofan has a low-bypass ratio; the F100 bypass ratio is $\beta = 0.71$. To compute the thrust of a pure turbojet, the bypass ratio is set to zero. The afterburner can be shut off by setting the stagnation temperature at the afterburner exit T_{06} equal to T_{05}, the stagnation temperature at the afterburner inlet, and by setting f_{ab}, the fuel-to-air ratio for the afterburner, equal to zero.

The model to be presented is not limited to any one programming language or mathematical toolkit. However, in the analysis that follows, all variables will be written with their arguments to illustrate how this model is implemented in Mathcad. A standard atmosphere model (not discussed here) is implemented such that when an altitude h is specified, the ambient temperature $T_a(h)$ and the ambient pressure $p_a(h)$ may be obtained. From these, the ideal-gas law is used to compute the density $\rho(h)$, and the speed of sound $a(h)$ is computed from

$$a(h) = \sqrt{\gamma R T_a(h)} \tag{2}$$

where $\gamma = 1.4$ is the ratio of specific heats for air, and $R = 1716\ \text{ft}^2/\text{s}^2 \cdot {}^\circ\text{R}$ is the gas constant for air. If the Mach number M is specified, then the inlet velocity $u(h, M)$ may be computed from $u(h, M) = Ma(h)$. The ambient stagnation temperature and pressure are computed from the standard expressions for isentropic flow:

Presented as Paper 1058 at the 45th AIAA Aerospace Sciences Meeting and Exhibit, Reno, NV, 8–11 January 2007; received 1 October 2007; revision received 3 December 2007; accepted for publication 26 December 2007.

*Associate Professor, Department of Aerospace Engineering, P. O. Drawer A. Associate Fellow AIAA.

$$T_{0a}(h,M) = T_a(h)\left[1 + \frac{\gamma - 1}{2}M^2\right],$$
$$p_{0a}(h,M) = p_a(h)\left[1 + \frac{\gamma - 1}{2}M^2\right]^{\frac{\gamma}{\gamma-1}} \tag{3}$$

The air enters the diffuser or inlet, which is assumed to cause losses in stagnation pressure but no losses in stagnation temperature. The stagnation temperature at the exit of the diffuser and the entrance to the compressor $T_{02}(h,M)$ is assumed to be equal to the ambient stagnation temperature, or $T_{02}(h,M) = T_{0a}(h,M)$. The stagnation pressure losses in the diffuser may be handled by a number of different means. Hill and Peterson [6] define a diffuser efficiency η_d that is described as being a strong function of Mach number. The approach presented here is to use the following ad hoc expression (developed by the author and a colleague) for the stagnation pressure at the diffuser exit/compressor entrance:

$$p_{02}(h,M) = p_{0a}(h,M)\left[1 - a_d\left(\frac{M}{b_d}\right)^2\right] \tag{4}$$

The values for the constants a_d and b_d were varied in an attempt to match the computed thrust variations with experimental data. The determination of these particular constants will be discussed in more detail later.

At this point in the analysis, certain engine parameters must be specified. These are shown in Table 1, which both defines the variable to be used and lists a typical value for each variable (see, for example, [6]). These variables are the pressure ratios across each component, the isentropic efficiency for each component, and the specific heat ratio.

The changes in specific heat ratios between the inlets and exits of the burner and the afterburner, in which the temperature changes are the highest, take into account the variations of the gas properties with temperature.

In addition to these properties, some additional properties for the burner and afterburner must be specified. These are listed in Table 2, which defines the stagnation temperatures at the exits of the burner and afterburner and the specific heats at the entrance and exit of each component and gives typical values. The changes in specific heats again take into account the variations of gas properties with temperature.

The engine parameters that can usually be found in references such as *Jane's All the World's Aircraft* are the compressor pressure ratio and the burner and afterburner stagnation temperatures. The stagnation temperatures are the highest temperatures in the engine and are typically limited by material properties. The other numbers shown are typical numbers given the typical temperature ranges in aircraft engines (see, for example, [6]). The final engine parameters that have to be specified are the inlet area A_i and the fuel heating value Q_R. The values used in the calculations that follow are $A_i = 5.0$ ft^2 and $Q_R = 19,000$ Btu/lbm (this value is close to that for JP4 jet fuel).

Given the engine parameters just discussed, the stagnation temperature and pressure at the compressor exit/burner inlet are computed from

$$T_{03}(h,M) = T_{02}(h,M)\left[1 + \frac{1}{\eta_c}(pr_c^{\frac{\gamma_c-1}{\gamma_c}} - 1)\right],$$
$$p_{03}(h,M) = p_{02}(h,M)pr_c \tag{5}$$

The stagnation temperature and pressure at the fan exit are computed from

$$T_{08}(h,M) = T_{02}(h,M)\left[1 + \frac{1}{\eta_f}(pr_f^{\frac{\gamma_f-1}{\gamma_f}} - 1)\right],$$
$$p_{08}(h,M) = p_{02}(h,M)pr_f \tag{6}$$

The stagnation temperature at the burner exit/turbine entrance, T_{04}, is set equal to its given value as shown in Table 2. The stagnation pressure at the burner exit/turbine entrance is computed from $p_{04}(h,M) = p_{03}(h,M)pr_b$. The fuel–air ratio for the main burner is computed from

$$f(h,M) = \frac{C_{p4}T_{04}(h,M) - C_{p3}T_{03}(h,M)}{\eta_b Q_R - C_{p4}T_{04}(h,M)} \tag{7}$$

The stagnation temperature at the turbine exit/afterburner inlet is computed from

$$T_{05}(h,M) = T_{04}(h,M)\left\{1 - \eta_t\left[1 - \left(\frac{p_{05}(h,M)}{p_{04}(h,M)}\right)^{\frac{\gamma_t-1}{\gamma_t}}\right]\right\} \tag{8}$$

and the stagnation pressure at the turbine exit/afterburner inlet is computed from

$$p_{05}(h,M) = p_{04}(h,M)\left[1 - \frac{C_p(T_{03}(h,M) - T_{02}(h,M)) + \beta C_p(T_{08}(h,M) - T_{02}(h,M))}{\eta_t[1 + f(h,M)]C_{p4}T_{04}(h,M)}\right]^{\frac{\gamma_t}{\gamma_t-1}} \tag{9}$$

The stagnation temperature at the afterburner exit/nozzle entrance is set to the specified value T_{06} as shown in Table 2. The stagnation pressure at the afterburner exit/nozzle entrance is computed from $p_{06}(h,M) = p_{05}(h,M)pr_{ab}$. The fuel–air ratio for the afterburner is computed from

Table 1 Definitions and typical values of engine component parameters

Component	Pressure ratio	Efficiency	Specific heat ratio
Compressor	$\text{pr}_c = 8.0$	$\eta_c = 0.88$	$\gamma_c = 1.4$
Fan	$\text{pr}_f = 1.5$	$\eta_f = 0.92$	$\gamma_f = 1.4$
Burner	$\text{pr}_b = 0.98$	$\eta_b = 0.98$	$\gamma_3 = 1.38$ (inlet) $\gamma_4 = 1.33$ (exit)
Turbine	Computed	$\eta_t = 0.95$	$\gamma_t = 1.35$
Afterburner	$\text{pr}_{ab} = 0.90$	$\eta_{ab} = 0.99$	$\gamma_5 = 1.35$ (inlet) $\gamma_6 = 1.3$ (exit)
Nozzle	Computed	$\eta_n = 0.99$	$\gamma_n = 1.35$

Table 2 Definitions and typical values of burner and afterburner parameters

	Burner	Afterburner
Stagnation temp. at exit	$T_{04} = 2800°\text{R}$	$T_{06} = 3700°\text{ R}$
Specific heat at entrance	$C_{p3} = 0.25$ Btu/lbm $\cdot\,°\text{R}$	$C_{p5} = 0.26$ Btu/lbm $\cdot\,°\text{R}$
Specific heat at exit	$C_{p4} = 0.27$ Btu/lbm $\cdot\,°\text{R}$	$C_{p6} = 0.30$ Btu/lbm $\cdot\,°\text{R}$

$$f_{ab}(h, M) = \frac{(1+\beta)C_{p6}T_{06}(h,M) - \beta C_p T_{08}(h,M) - C_{p5}T_{05}(h,M)}{\eta_{ab}Q_R - C_{p6}T_{06}(h,M)} \tag{10}$$

The pressure at the nozzle exit is assumed to be matched to atmospheric pressure for most efficient engine operation. The nozzle exit velocity is computed from

$$u_e(h,M) = \sqrt{2\frac{\gamma_n}{\gamma_n - 1}RT_{06}(h,M)\eta_n\left[1 - \left(\frac{p_a(h)}{p_{06}(h,M)}\right)^{\frac{\gamma_n - 1}{\gamma_n}}\right]} \tag{11}$$

The end result is that the thrust is the product of the mass flow rate through the engine times the change in velocity through the engine, or

$$T(h,M) = \dot{m}_{\text{air}}(h,M)[(1 + f(h,M) + f_{ab}(h,M))u_e(h,M) - u(h,M)] \tag{12}$$

What is problematic in Eq. (12) is the mass flow rate of air entering the engine, or $\dot{m}_{\text{air}}$. In the presentation by Hill and Peterson [6], this mass flow rate is simply taken as ρuA, the product of the density at a given altitude, the flight speed of the aircraft, and the inlet area for the engine. One problem with this assumption is that it predicts zero static thrust (the thrust at zero Mach number). This assumption also does not take into account the variation of the capture area, or the effective area of the flow entering the engine, as a function of Mach number. At high subsonic and at supersonic Mach numbers, the deceleration of the air as it enters the engine causes a significant change in the effective area of the stream tube that enters the engine at freestream conditions. Not taking into account this Mach number effect has a significant impact on the values of thrust computed using the model.

The difficulty in predicting the mass flow rate of air into the engine was circumvented using data available in the classic aircraft design book by Nicolai [7]. Nicolai presented the required air mass flow rate for an F-100 engine as a function of Mach number for several different altitudes. These curves are shown in Fig. 1 (Fig. 14.7h in [7]). Among other things, these curves show the mass flow required at zero Mach number, thus allowing for a nonzero static thrust value. The curves shown in Fig. 1 were digitized, and each curve was normalized by the density at the given altitude for each curve (assuming a standard atmosphere), the speed of sound at each altitude (also from a standard atmosphere), and the reference area for the engine. The resulting data points collapsed remarkably well onto a single curve, as shown in Fig. 2. A polynomial curve fit applied to this set of data yielded the following result for the mass flow rate of air as a function of altitude and M:

$$\dot{m}_{\text{air}}(h,M) = \rho(h)a(h)A_i Q^*(M) \tag{13}$$

where

$$Q^*(M) = 0.4217 + 0.2643M^2 + 0.01995M^4 \tag{14}$$

A polynomial in even powers of the Mach number was chosen deliberately so that the $Q^*(M)$ function would be monotonic. The inlet area A_i is obtained from reference materials such as *Jane's All the World's Aircraft* and is then adjusted by the user so that the sea-level static thrust for a particular aircraft is matched to the value usually found in a reference such as *Jane's*.

A comparison of the thrust curves generated by the model with data for the F100 engine from Nicolai [7] is shown in Fig. 3. For these calculations, the values of the constants in Eq. (4) were $a_d = 0.95$ and $b_d = 3.4$. These values were chosen in an attempt to match the thrust and drag variations with Mach number and altitude exhibited by the experimental data. The agreement between the model and data points can only be described as fair. The model underpredicts the thrust at low M and overpredicts the thrust at high M, although it does

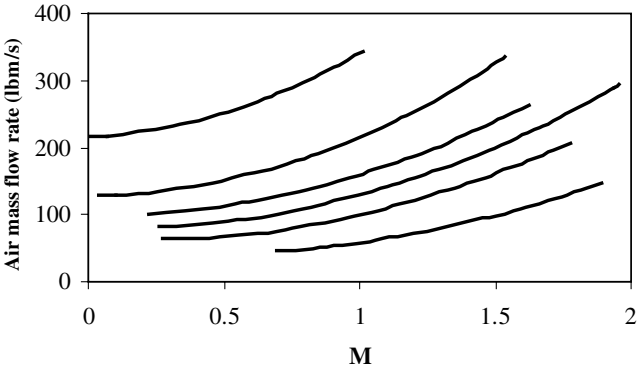

Fig. 1 Required air mass flow rates for an F-100 engine; top to bottom, curves correspond to altitudes of 0, 15,000, 25,000, 30,000, 36,000, and 45,000 ft (data from Fig. 14.7h in [7]).

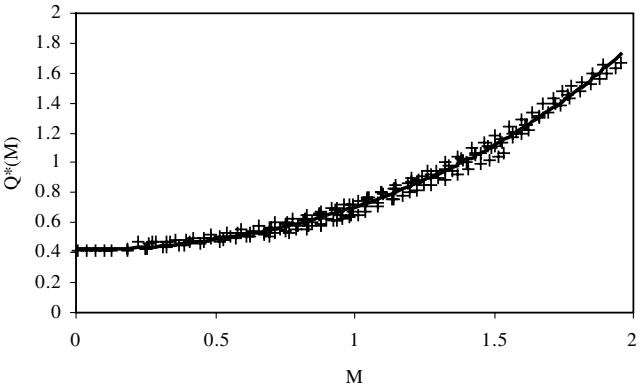

Fig. 2 Dimensionless air mass flow rate as a function of Mach number.

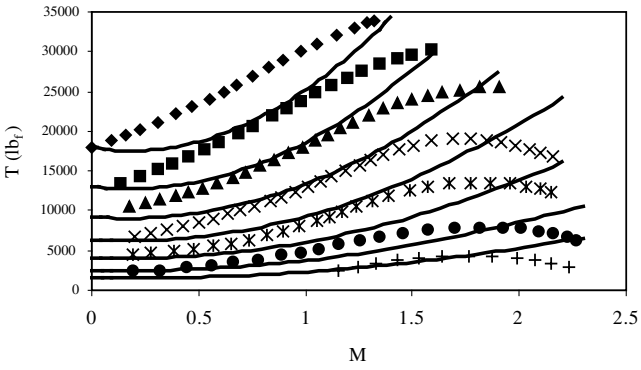

Fig. 3 Comparison of thrust model predictions and thrust data from [7]; solid curves are computed thrust values and points are test data at altitudes beginning at sea level (the top set of points) and extending to 60,000 ft in increments of 10,000 ft.

a slightly better job at higher altitudes. At most, it roughly captures the trends in the data. However, the model is not totally useless. Figure 4 shows a comparison of the thrust predicted by the model (normalized by the sea-level static thrust) with data available from Bryson and Ho [8]. The specific engine is not identified, and little information is given along with the data in [8]. A pure turbojet with afterburner was assumed, and the inlet area was adjusted so that the reported sea-level static thrust value of 23,500 lbf was obtained. The dimensionless air mass flow rate function $Q^*(M)$ given by Eq. (14) was used without change. Initially, the thrust values were compared with the data from [8] using the values of the parameters a_d and b_d for the F100 engine, used to generate Fig. 3. When it was observed how well the values from the thrust model agreed with the data from [8] (shown in Fig. 4), the values of a_d and b_d were modified to improve

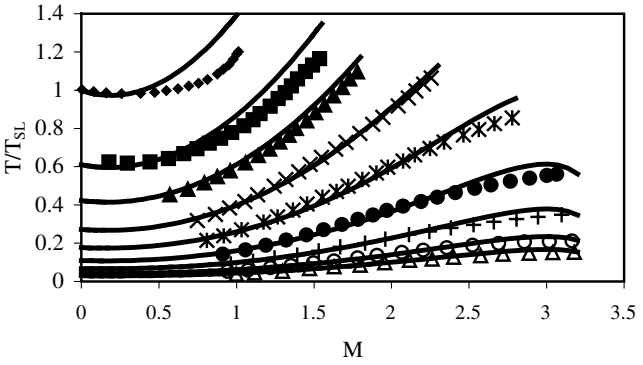

Fig. 4 Comparison of thrust model predictions and thrust data of [8]; solid curves are computed values and points are test data at altitudes of 0 (top set), 15,000, 25,000, 36,089, 45,000, 55,000, 65,000, 75,000, and 82,021 ft (bottom set); SL denotes sea level.

the agreement with the data from [8], resulting in $a_d = 0.85$ and $b_d = 3.2$. These were the values used to generate the solid curves shown in Fig. 4. As a check, the curves for the F100 engine were recomputed using these values of a_d and b_d, and the differences in the curves were almost undetectable.

The model presented by Hill and Peterson [6] and implemented here along with the mass flow rate model also computes the thrust-specific fuel consumption (TSFC). The mass flow rate of the fuel is first computed from

$$\dot{m}_f(h, M) = \dot{m}_{\text{air}}(h, M)[f(h, M) + f_{ab}(h, M)] \tag{15}$$

and then the TSFC or $c(h, M)$ is computed from

$$\text{TSFC}\,(h, M) = c(h, M) = \frac{\dot{m}_f(h, M)}{T(h, M)} \tag{16}$$

An example of those calculations is shown in Fig. 5. The agreement between the computed TSFC curves and experimental data for the F100 engine shown in Fig. 5a appears to be similar to the agreement between the measured and predicted thrust curves (Fig. 3). Data for TSFC from Nicolai [7] tend to start high, have a relative minimum in the mid-Mach-number range, and then increase as M increases, whereas the model values tend to start low, plateau in the mid-Mach-number range, and then increase, as shown in Fig. 5a. Where the data and the model do agree, at least to a certain degree, is in the collapse to a single curve for altitudes greater than 36,089 ft. The curves in Fig. 5b were computed for the pure turbojet (Fig. 4), for which no TSFC data were available for comparison.

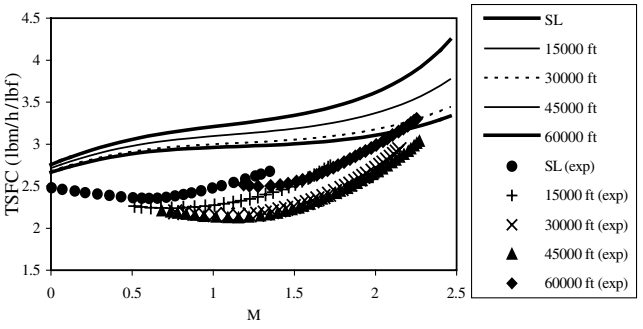

a) F100 engine (experimental data from [7])

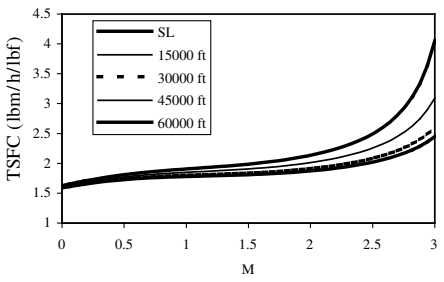

b) Pure turbojet

Fig. 5 TSFC curves for the F100 engine of Fig. 3 and for the pure turbojet of Fig. 4 computed from the thrust model (note that in the model, all curves collapse to the bottom curve for altitudes greater than 36,089 ft); SL denotes sea level.

It would appear that even though the dimensionless mass flow rate function $Q^*(M)$ was obtained from the data for a specific engine, it does a reasonably good job of predicting the performance of other engines as well. It would also appear that the thrust model used here is better suited for simpler engines such as pure turbojets and not so much for complicated engines, such as the low-bypass augmented turbofan. The model does, however, have the added virtue in that it is identical to a model developed in an undergraduate aircraft propulsion course, meaning that it reinforces and is reinforced by instruction in two different classes.

It is recognized that there are higher-fidelity thrust models available (in particular, see the book by Mattingly et al. [9]). However, the current model is relatively simple and seems to provide reasonable predictions of thrust behavior with Mach number and altitude. Its primary value lies in the fact that when all of the procedures are implemented properly, then thrust and TSFC become readily available functions of altitude and Mach number. This is particularly useful when performing these calculations in Mathcad, because it allows for the specification of a function for thrust $T(h, M)$ and a function for TSFC $c(h, M)$ that can then be used easily in other calculations. Examples of these will be given later.

III. Drag Model

As discussed before, the basis for most drag calculations in performance analysis is the parabolic drag polar, given by Eq. (1). It is well known that both of the parameters needed in the drag model, the zero-lift drag coefficient C_{D0} and the induced-drag factor k, are functions of Mach number for values of M greater than about $M = 0.6$. What is less well known, at least in terms of available data, is how these parameters vary with M for specific aircraft. Again, Nicolai [7] provides useful data in this regard. Figures 6 and 7 (Figs. E.6 and E.7 from [7]) show the variation of the zero-lift drag coefficient with Mach number for various high-performance aircraft, some designed to fly supersonic (as in Fig. 6) and others designed purely as subsonic aircraft (such as shown in Fig. 7). Figure 8 (Fig. E.8 in [7]) shows the variation of k with Mach number for various aircraft configurations. It should be noted in this figure that only the data for the T-38 are shown for $M > 1$. In general, these data are much harder to obtain. Figure 9 (Fig. E.5 in [7]) shows the variation of k with M for various wing–body combinations with delta planforms.

An examination of the C_{D0} data in Fig. 6 shows that the data would probably be modeled well with a hyperbolic tangent function. An example of such a fit is shown in Fig. 10a, in which the function

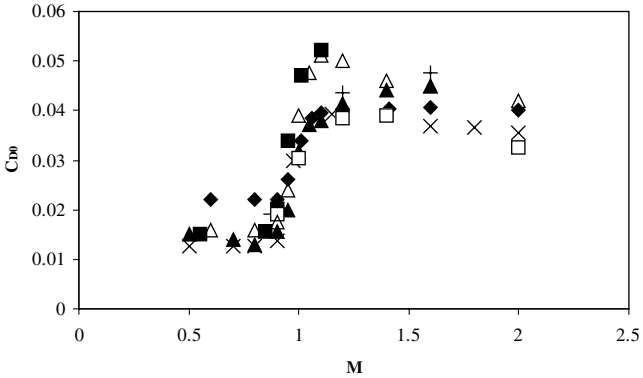

Fig. 6 Zero-lift drag coefficient data from Nicolai [7] (Fig. E.6) for supersonic aircraft: △ F-104G, ◆ F-4E, ■ A-7D, ▲ T-38, □ Northrop P600 (YF-17), + General Dynamics model 40 (YF-16), and × F-8J.

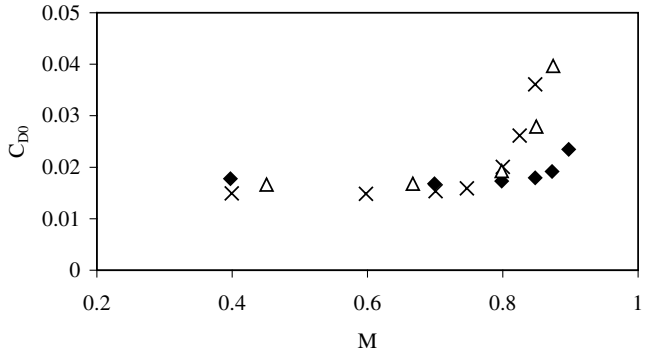

Fig. 7 Zero-lift drag coefficient data from Nicolai [7] (Fig. E.7) for subsonic aircraft: ◆ B-727, × C-141, and △ C-5A.

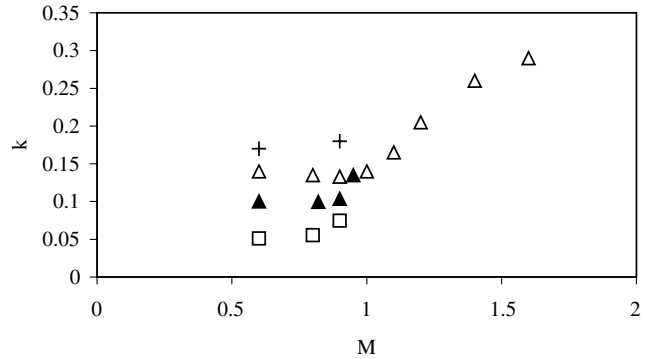

Fig. 8 Induced-drag factor k for various aircraft from Nicolai [7] (Fig. 3.8): △ T-38, □ B-727, ▲ A-7D, and + F-4C.

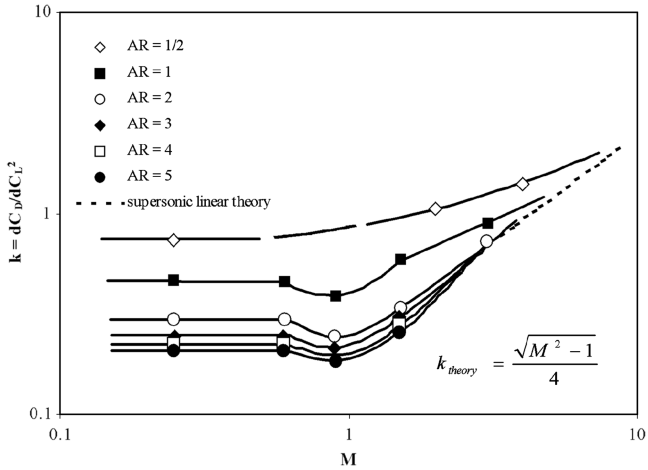

Fig. 9 Induced-drag factor k data for wing–body combinations with delta planforms from Nicolai [7] (Fig. E.5); A denotes the aspect ratio.

$$C_{D0}(M) = A_D + B_D \tanh[C_D(M - D_D)] \tag{17}$$

was fit to the data obtained from Fig. 6 for the T-38. The fit values were $A_D = 0.028$, $B_D = 0.015$, $C_D = 12.201$, and $D_D = 0.992$. The hyperbolic tangent function does a good job in general of fitting the data to transonic aircraft for which the value of C_{D0} (at least to the extent that the data are reported) does not decrease for $M > 1$ (an example of an even better fit is shown in Fig. 10b for the F-4C). For some of the aircraft shown in Fig. 7, C_{D0} does decrease as M increases above $M = 1$. For aircraft such as this, the fit given by Eq. (17) is modified as follows:

$$C_{D0}(M) = A + \frac{B \tanh[C(M - D)]}{1 + EM^n} \tag{18}$$

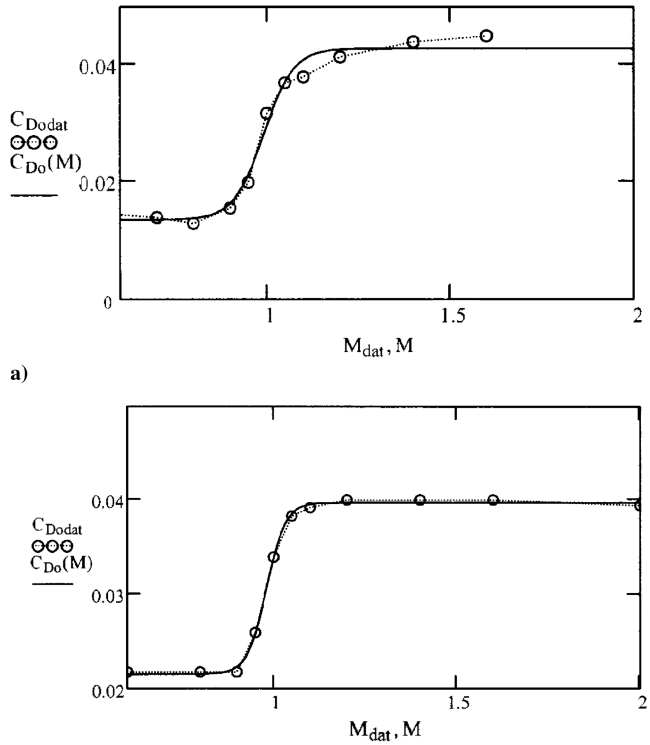

Fig. 10 Examples of hyperbolic tangent curve fits to zero-lift drag coefficient data from Nicolai [7]: a) T-38 and b) F-4C.

The values of E and n are usually adjusted simply to provide a reasonable decrease in the zero-lift drag coefficient with supersonic Mach number. No real attempts were made to fit these parameters because of the paucity of available data.

The fit for $k(M)$ is a little more complicated. As both Figs. 8 and 9 show for a variety of configurations, k is constant for low Mach number, tends to dip around $M = 1$, and then increases, asymptotically approaching the value

$$k(M) = \frac{\sqrt{M^2 - 1}}{4} \tag{19}$$

This means that the slope of $k(M)$ is zero for low Mach numbers and asymptotically approaches $\frac{1}{4}$ for large Mach numbers. A hyperbolic tangent function was used for the slope of $k(M)$, because it could be made to vary gradually from a value of 0 at low M to a value of $\frac{1}{4}$ for large M. This function was then integrated to obtain the basic function for $k(M)$. An exponential function factor was added to produce the dip around $M = 1$. The resulting function for $k(M)$ is given by

$$k(M) = A_k + \left\{\frac{M}{8} + \frac{1}{8B_k}\ell_n\{\cosh[B_k(M - E_k)]\}\right\} \times [1 - C_k e^{-D_k(M-E_k)^2}] \tag{20}$$

This function was fit manually to the data from Nicolai [7] for the F-5/T-38 shown in Fig. 8. The data values and fitted curve are shown in Fig. 11. The values for the constants were $A_k = 0.021$, $B_k = 15.0$, $C_k = 0.056$, $D_k = 7.0$, and $E_k = 0.99$. These were adjusted to obtain a reasonable value for the zero Mach number value for k and to provide a shape that agreed in general with reported observations. Again, more serious attempts to fit the data were not made because of the paucity of available data.

With models in hand for $C_{D0}(M)$ and $k(M)$, the drag itself can be computed as a function of altitude and Mach number. Using the dimensionless wing-loading parameter $\omega(h)$ defined by

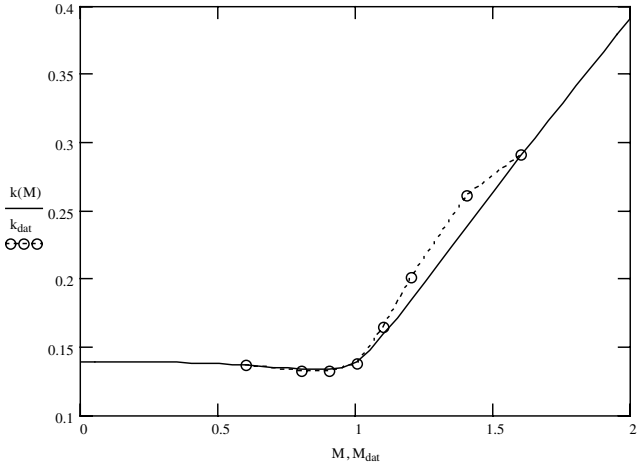

Fig. 11 Illustration of the fit of Eq. (20) to induced-drag parameter k data for F-5/T-38; solid line is the fit and points are data from Nicolai [7] (see Fig. 8).

$$\omega(h) = \frac{2W}{\gamma p(h) S} \tag{21}$$

where W is the aircraft weight, γ is the ratio of specific heats, $p(h)$ is the pressure at a given altitude obtained from a standard atmosphere model, and S is the aircraft reference wing area, the drag-to-weight ratio at a given altitude and Mach number may be computed from

$$\frac{D(h,M)}{W} = C_{D0}(M)\frac{M^2}{\omega(h)} + k(M)\frac{\omega(h)}{M^2} \tag{22}$$

This function may then be implemented in Mathcad, and drag as a function of altitude and Mach number may be computed easily.

IV. Applications

A. Cruise Mach Number and Ceiling Calculations

The aircraft to be used in this and subsequent examples, unless otherwise noted, is the F-5/T-38, because Nicolai [7] provides values for both C_{D0} and k values into the supersonic range (see Figs. 6 and 8). The other necessary data were obtained from the 1983–1984 edition of *Jane's* [10] for the Northrop F-5E Tiger II.

The use of the thrust and drag models allows for the easy calculation of the cruise Mach number and the absolute ceiling for a given aircraft. Figure 12 is an example of the determination of the cruise Mach number for the F-5/T-38. When thrust and drag are expressed as functions of altitude and Mach number, it is very easy in Mathcad to set the altitude and then determine the Mach number at which $T(h, M) = D(h, M)$, using a root function or a given-find block. The fact that the transonic drag rise effects are included in the drag function means that realistic values for the cruise Mach number are obtained. For the calculations shown in Fig. 12, the intake area was adjusted until the static sea-level thrust with afterburner matched the reported value in [10] of 10,000 lbf. This was the only variable adjusted in the thrust model. The altitude was set to $h = 36,000$ ft and the weight was set to $W = 13,350$ lbf, the reported combat weight of the F-5E. The result was a maximum cruise Mach number of $M = 1.535$, which agrees reasonably well with the value of $M = 1.64$ reported in [10] (the reported value for the F-5F is 1.56).

Figure 13 is an example of a ceiling calculation. The absolute ceiling for an aircraft occurs when the thrust is equal to the drag at a single point. Again, this is easily done in Mathcad. The altitude is manually adjusted until the curves intersect at a single point, and the root function or given-find block is used to determine the intersection point. In this example, the ceiling for the F-5E was determined to be 55,700 ft at a Mach number of 0.934. The same model was used to compute the service ceiling for the F-5E by computing the rate of climb as a function of altitude and Mach number and setting it equal to 100 ft/ min. The resulting value of 55,500 ft is not unreasonably different from the value of 51,800 ft for the service ceiling of the F-5E as reported by [10].

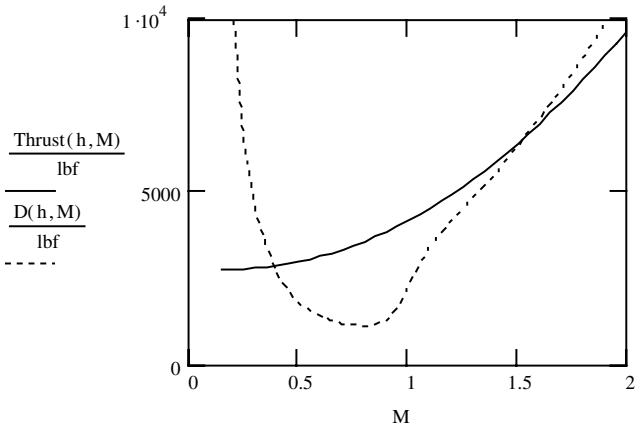

Fig. 12 Example of using thrust and drag models in Mathcad to determine cruise Mach number for F-5E at 36,000 ft.

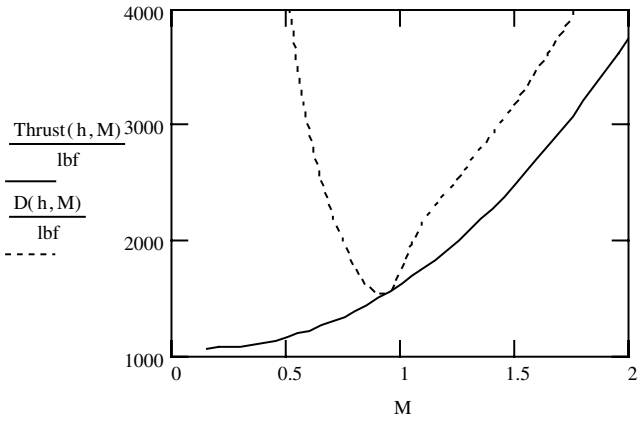

Fig. 13 Example of use of thrust and drag models in Mathcad to determine the absolute ceiling for F-5E.

B. Range Calculations

Vinh [3] presented an analysis of range performance in which the maximum range for an aircraft occurs at the Mach number for which the function $G(M, h)$ is maximized, where $G(M, h)$ is given by

$$G(M,h) = \frac{M^{1/b(h)} E_{\max}(M)}{c(h,M)(C_L^*(M))^{\frac{b(h)-1}{2b(h)}}}$$
$$E_{\max}(M) = \frac{1}{2\sqrt{k(M)C_{D0}(M)}}, \qquad C_L^*(M) = \sqrt{\frac{C_{D0}(M)}{k(M)}} \tag{23}$$

In these equations, $b(h)$ is an exponent in the standard atmosphere model, with $b(h) = 1.235$ in the troposphere and $b(h) = 1$ in the stratosphere. Figure 14 shows $G(h, M)$ plotted as a function of Mach number for two different altitudes, one in the troposphere and one in the stratosphere, for the F-5/T-38. For this particular aircraft, the function G has relative maxima at subsonic and supersonic Mach numbers in both the troposphere and the stratosphere. According to Vinh's [3] procedure, the Mach numbers are then checked using the equation

$$\frac{p}{p_*} = \delta(h) = \frac{2\sqrt{W_1 W_2}}{\gamma p_* S}\frac{d(h)}{M^2 C_L^*(M)} \tag{24}$$

In this equation, the asterisk subscript indicates a condition at the tropopause. The function $d(h)$ appears in the analysis by Vinh [3] and has a value of 1.1 in the troposphere and 1 in the stratosphere. The

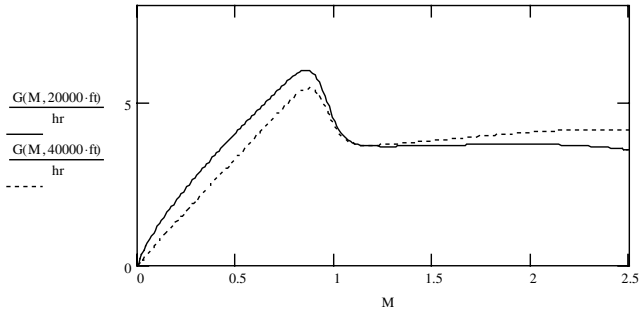

Fig. 14 Function $G(M, h)$ as defined by Vinh [3] for use in maximum-range calculations.

ratio $\delta = p/p_*$ is the ratio of the pressure at some altitude to the pressure at the tropopause, and so the Mach numbers obtained in maximizing G in Eq. (23) should produce a value of δ greater than 1 in the troposphere and less than 1 in the stratosphere. This procedure allows for the rejection of spurious solutions. For legitimate values of $M = M_{\text{opt}}$ and the corresponding values of δ, the standard atmosphere equations may be inverted to yield h_{opt}, the optimum altitude(s) for cruise. Under the restrictions of constant-Mach-number, constant-lift-coefficient cruise used in the analysis by Vinh, two range calculations may be made using the legitimate Mach number values obtained. The cruise-climb range in the stratosphere may be computed from

$$R = a_* G(M_{\text{opt}}, h_{\text{opt}})\, \ell_n\left(\frac{1}{1-\zeta}\right) \tag{25}$$

where $\zeta = \Delta W_f / W_1$ is the cruise-fuel weight fraction. The range for constant-altitude, constant-velocity cruise may be computed from

$$R = 2a_* \frac{ME_{\max}(M)}{c(h,M)} (\delta(h,M))^{\frac{b(h)-1}{2b(h)}} \tan^{-1}\left[\frac{d(h)\zeta}{[1+(d(h))^2]\sqrt{1-\zeta}}\right] \tag{26}$$

In these expressions, the values for M_{opt} and h_{opt} are used.

For the sample calculations shown in Fig. 14, an empty weight of 10,000 lbf was assumed. According to [10], the maximum internal fuel capacity is 2563 l (677 gal). This, along with an assumed fuel density of 800 kg/m^3 = 1.552 slug/ft^3, was used to compute a cruise fuel weight of ΔW_f of 4500 lbf, yielding a cruise-fuel-weight fraction of $\zeta = 0.31$. These values for the weights yielded the values for the range parameters shown in Table 3.

The two solutions in the troposphere are invalid because they yield values of $\delta < 1$. The valid values of δ were then used to compute the corresponding altitudes, revealing that the supersonic solution for optimum range would occur at an altitude of over 81,000 ft, well above the absolute ceiling for the F-5. Of course, there is the more fundamental problem with the supersonic solution in that the required Mach number exceeds the maximum possible Mach number for the F-5/T-38 significantly (there are no thrust limitations in the analysis by Vinh [3]). The corresponding altitude for the subsonic solution in the stratosphere was $h_{\text{opt}} = 41,450$ ft, well within the realm of possibility for the F-5/T-38. The cruise-climb range computed from Eq. (25) was 1334 miles, and the constant-altitude, constant-velocity range computed from Eq. (26) was 1326 miles. The maximum ranges reported in [10] are 1543 miles with drop tanks retained and 1779 miles with drop tanks jettisoned.

Table 3 Results of optimum range calculations for F-5/T-38

Altitude h	M_{opt}	$G(M_{\text{opt}}, h)$, h	$\delta(M_{\text{opt}}, h)$	Valid solution?
20,000 ft	0.856	5.99	0.887	No
20,000 ft	1.93	3.72	0.167	No
40,000 ft	0.868	5.44	0.775	Yes
40,000 ft	2.38	4.17	0.114	Yes

The range calculations presented here assumed only internally carried fuel was burned, and so it is not surprising that the ranges came out low compared with the values from [10]. If more of the specifics of the mission profiles for which the maximum ranges were reported in [10] were included in the analysis, it is likely that the numbers could be matched more closely. The example here was done simply to illustrate that the thrust and drag models described provide reasonable results when used with the range calculation procedures as presented by Vinh [3].

C. Energy Methods

One of the earliest methods of performance analysis developed primarily for high-performance aircraft was the group of techniques referred to collectively as energy methods [4,5]. The use of energy methods allows for the determination of climbs to given final energy states that minimize time or fuel burn and also glides that maximize range. The total energy per unit weight is expressed as an equivalent energy height, given by

$$h_e(h, M) = h + \frac{V^2}{2g} = h + \frac{[Ma(h)]^2}{2g} \tag{27}$$

The time rate of change of the equivalent energy height is given by

$$\frac{\mathrm{d}h_e}{\mathrm{d}t}(h, M) = \frac{P_{ex}(h, M)}{W} = \frac{[T(h, M) - D(h, M)]Ma(h)}{W} = p_{\text{ex}}(h, M) \tag{28}$$

According to the theory of energy methods, at a particular equivalent energy height h_e, the maximum rate of change of h_e (and hence the ability to climb to the next highest energy level in the minimum amount of time) occurs at that combination of altitude and Mach number at which a curve of constant $\mathrm{d}h_e/\mathrm{d}t$ is tangent to the curve of constant $h_e(h, M)$ of the given value in the altitude–Mach-number plane. The complete set of tangency points, along with zoom climbs and zoom dives along contours of constant h_e, trace out a trajectory in altitude and Mach number. The actual time to climb to the final energy state can be determined from a numerical evaluation of the integral

$$t = \int_{h_{e1}}^{h_{e2}} \frac{\mathrm{d}h_e}{\mathrm{d}h_e/\mathrm{d}t} = \int_{h_{e1}}^{h_{e2}} \frac{\mathrm{d}h_e}{p_{\text{ex}}} \tag{29}$$

Note that the constant-energy climbs and dives do not contribute to the integral, because along those portions of the trajectory, $\mathrm{d}h_e = 0$. By evaluating the function $\mathrm{d}h_e/\mathrm{d}t$ at the Mach numbers and altitudes from the tangency points on the trajectory, the total time to climb to the final specified energy state may be obtained. An example of such a trajectory determination is shown in Fig. 15. The ability to specify thrust and drag as functions of altitude and Mach number make these calculations particularly straightforward in Mathcad, except in one respect. The author generally prefers the contour plotting capabilities of MATLAB, and so Mathcad is used to generate values of the necessary quantities on an altitude–Mach-number grid. These values are then imported into MATLAB to generate the required contour plots, such as those shown in Fig. 15. All of the actual computations are performed in Mathcad.

The contours shown in Fig. 15 were generated for the F-5/T-38 using the values in the preceding thrust and drag models. Contours of constant specific excess power p_{ex} are overlaid on contours of constant specific energy height h_e evaluated at 5000-ft intervals. The final state for the minimum-time climb shown in Fig. 15 was an altitude of 35,000 ft and a Mach number of 1.5 and is indicated by a circle in Fig. 15. This corresponded to a final energy level of $h_e = 68,100$ ft, which is the value of the h_e contour passing through the final state. The contour plot was read using a digitization program and the tangency points on the minimum-time trajectory were selected. This trajectory is illustrated in Fig. 15. It is essentially a constant-Mach-number climb to altitude, followed by a constant-energy dive through $M = 1$, and then an acceleration to the final energy level, followed by a short constant-energy dive to get to the

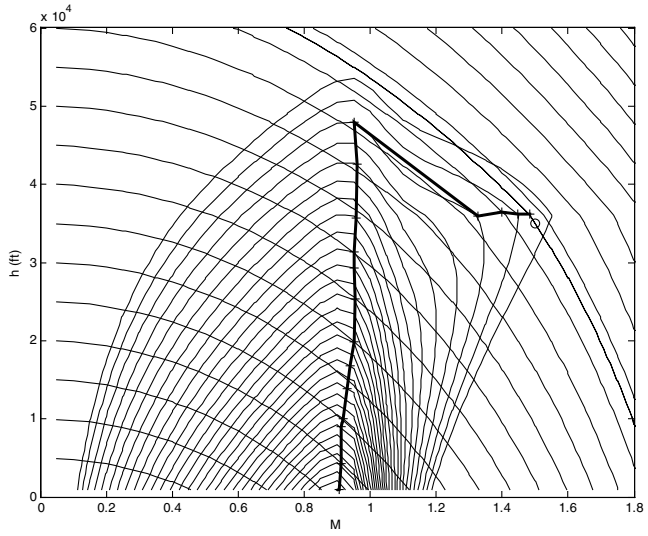

Fig. 15 Contours of constant specific energy h_e and constant specific excess power per unit weight p_{ex} for use in energy methods to determine a minimum-time climb trajectory.

final required altitude and Mach number. The points on the trajectory were entered into the Mathcad worksheet and the integrand in Eq. (29) was evaluated at each of the points on the trajectory. The results of these evaluations are shown plotted against the energy height h_e in Fig. 16. The area under this curve is the total time to climb to the final energy state. For this particular example, the total time was approximately 9.0 min.

Another type of climb that may be optimized using energy methods is a minimum-fuel-burn climb. The rate of change of energy height h_e with respect to change in fuel weight W is given by

$$\frac{\mathrm{d}h_e}{\mathrm{d}W} = \frac{\mathrm{d}h_e}{\mathrm{d}t}\frac{\mathrm{d}t}{\mathrm{d}W} = p_{\mathrm{ex}}(h,M)\left(\frac{1}{-c(h,M)T(h,M)}\right) = -\frac{p_{\mathrm{ex}}(h,M)}{c(h,M)T(h,M)} \tag{30}$$

As before, at a particular equivalent energy height h_e, the maximum rate of change of h_e for a given amount of fuel burned (and hence the ability to climb to the next highest energy level with the minimum amount of fuel burned) occurs at that combination of altitude and Mach number at which a curve of constant $\mathrm{d}h_e/\mathrm{d}W$ is tangent to the curve of constant $h_e(h,M)$ of the given value in the altitude–Mach-number plane. The weight of fuel burned may be determined by evaluating the integral

$$\Delta W = \int_{h_{e1}}^{h_{e2}} \frac{\mathrm{d}h_e}{\mathrm{d}h_e/\mathrm{d}W} = -\int_{h_{e1}}^{h_{e2}} \frac{cT}{p_{ex}}\,\mathrm{d}h_e \tag{31}$$

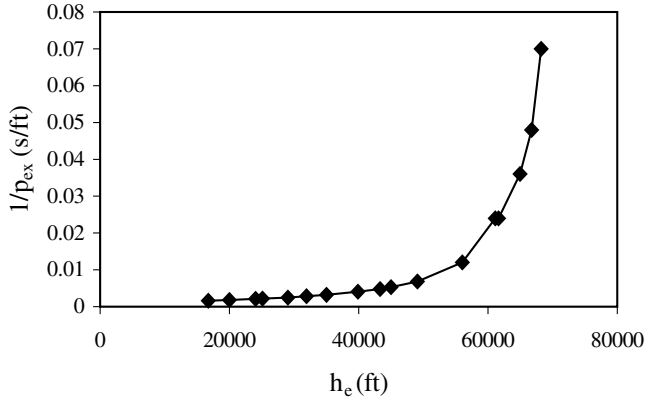

Fig. 16 Integrand of time-to-climb integral for minimum-time climb; total time to climb is the area under the curve.

In this integral, the minus sign simply reflects the fact that the change in fuel weight is negative, because fuel is burned during the climb, and therefore may be neglected. An example of a minimum-fuel-burn climb calculation for the F-5/T-38 is shown in Figs. 17 and 18. Figure 17 shows the contours of constant $\mathrm{d}h_e/\mathrm{d}W$ as given by Eq. (30) overlaid on the contours of constant h_e. The final altitude and Mach number were 35,000 ft and 1.5, respectively, as in the previous example. As before, the contour plot was read using a digitization program and the tangency points on the minimum-fuel-burn trajectory were selected. The resulting trajectory, shown in Fig. 17, is essentially a constant-Mach-number climb to altitude, followed by a constant-energy dive through $M = 1$, and then a constant-altitude acceleration to the final required energy level, followed by a constant-energy dive to the final required altitude and Mach number. It is interesting to note that the constant-altitude acceleration occurs at approximately 36,100 ft, which is essentially the altitude of the tropopause, indicating the maximum relative efficiency of the engine at that altitude. The points on the trajectory were entered into the Mathcad worksheet and the integrand in Eq. (31) was evaluated at each of the points on the trajectory. The results of these evaluations are shown plotted against the energy height h_e in Fig. 17. The area under this curve is the total fuel burned during the climb to the final energy state. For this particular example, the total fuel burned was approximately 1420 lbf. The vertical jump at $h_e = 60,000$ ft corresponds to the constant-energy dive through $M = 1$ and is the result of moving from a contour with one value of $\mathrm{d}h_e/\mathrm{d}W$ to a contour with a different value of $\mathrm{d}h_e/\mathrm{d}W$. During this

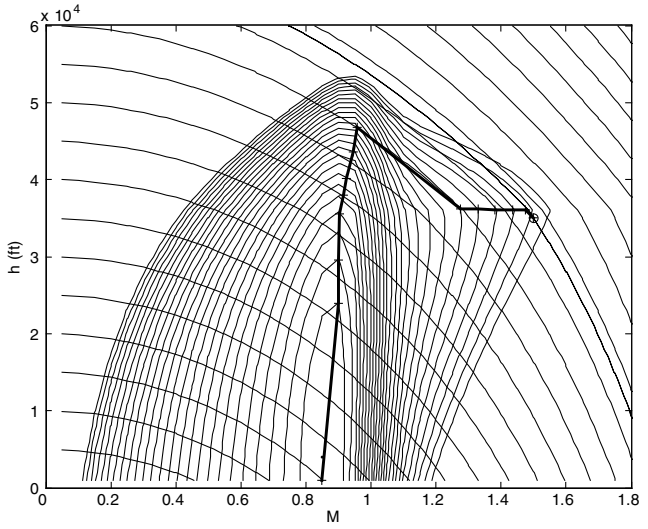

Fig. 17 Contours of constant specific energy h_e and constant $\mathrm{d}h_e/\mathrm{d}W$ for use in energy methods to determine a minimum-fuel-burn climb trajectory.

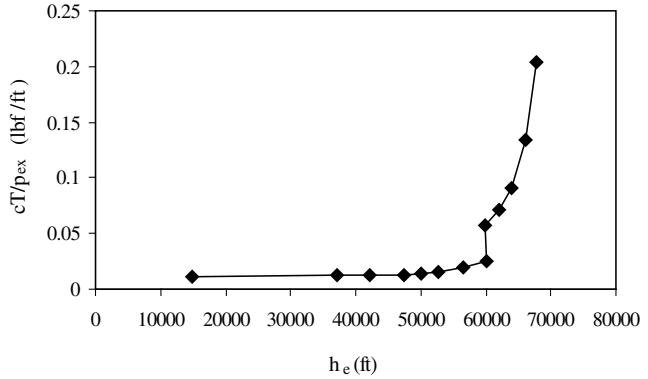

Fig. 18 Integrand of the time-to-climb integral for minimum-fuel-burn climb; total fuel burned during the climb is the area under the curve.

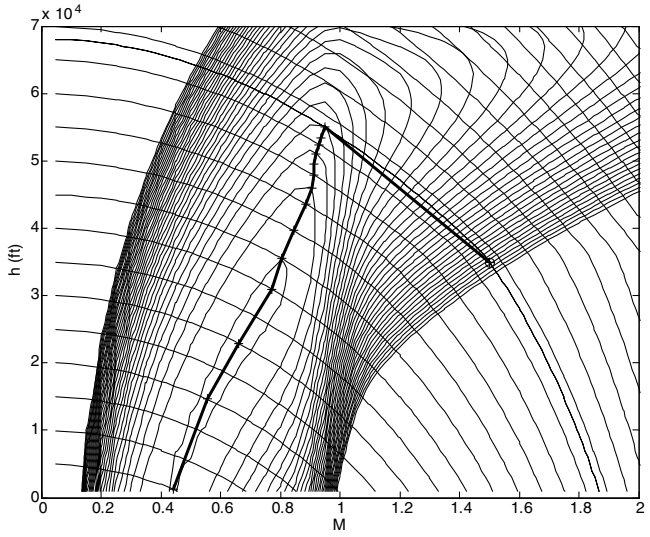

Fig. 19 Contours of constant specific energy h_e and constant $\mathrm{d}h_e/\mathrm{d}X$ for use in energy methods to determine a maximum-range glide trajectory (note that the first portion of the trajectory, the constant-energy zoom climb, is actually along the h_e contour and not along the straight line).

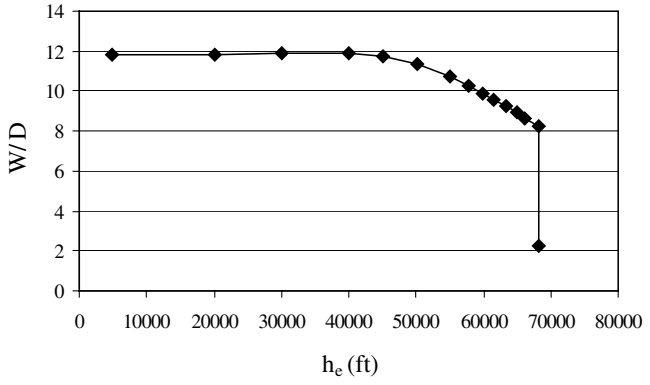

Fig. 20 Integrand of the range integral for maximum-range glide; total range during glide is the area under the curve.

dive, the energy height h_e does not change, and so there is no contribution to the integral during this segment of the climb. A dive through $M = 1$ along a constant-energy contour that maintains the value of $\mathrm{d}h_e/\mathrm{d}W$ would probably yield a better result. Such an approach was taken in the example of the minimum-time climb shown in Figs. 15 and 16.

A third flight path that may be optimized using energy methods is gliding flight from some altitude and Mach number. With the thrust equal to zero, the result for the instantaneous rate of change of energy height with forward distance is

$$\frac{\mathrm{d}h_e}{\mathrm{d}X} = -\frac{D(h, M)}{W} \tag{32}$$

The points at which the contours of constant $\mathrm{d}h_e/\mathrm{d}W$ are tangent to the contours of constant h_e are the points on the trajectory at each equivalent energy height at which the change in energy height is the smallest for a given forward-flight distance. The maximum-range glide trajectory is determined from these points. The total range is then computed from

$$\Delta X = -\int_{h_{e1}}^{h_{e2}} \frac{\mathrm{d}h_e}{\mathrm{d}h_e/\mathrm{d}X} = -\int_{h_{e1}}^{h_{e2}} \frac{W}{D}\,\mathrm{d}h_e = \int_{h_{e2}}^{h_{e1}} \frac{W}{D}\,\mathrm{d}h_e \tag{33}$$

Figures 19 and 20 show an example of a maximum-range glide for the F-5/T-38. In Fig. 19, the curves of constant D/W are overlaid on the curves of constant h_e. The initial flight condition is $h = 35,000$ ft and $M = 1.5$. The trajectory begins with a constant-energy zoom climb to the appropriate value of D/W and then follows the tangency points down to the final point, which was taken to be $M = 0.45$, with h close to zero. The integrand of Eq. (33) was evaluated at each point on the trajectory and the resulting values are shown in Fig. 20. The range is the area under this curve and, for this example, the maximum glide range was approximately 135 miles.

V. Conclusions

Simple but reasonably realistic models of thrust and drag as functions of altitude and Mach number were presented. Their implementation in a computational toolkit such as Mathcad and the ability to perform realistic performance calculations using these models were demonstrated. The thrust and drag models were used to predict cruise Mach number, absolute ceiling, and range for high-speed aircraft, as well as to determine minimum-time and minimum-fuel-burn climb trajectories and maximum-range glide trajectories. The values obtained in these examples were not necessarily *the* optimum performance values for the F-5/T-38. Rather, they were presented simply to illustrate the use of the thrust and drag models.

Acknowledgments

The author would like to acknowledge Keith Koenig of the Department of Aerospace Engineering at Mississippi State University for his assistance in the original development of the thrust model algorithm. The author would also like to acknowledge former students in his Advanced Performance class, particularly Viva Austin and K. Erin Wahlers, for introducing the author to the powers of Mathcad.

References

[1] Hale, F. J., *Introduction to Aircraft Performance, Selection, and Design*, Wiley, New York, 1984.

[2] Anderson, J. D., *Aircraft Performance and Design*, McGraw–Hill, New York, 1999.

[3] Vinh, N. X., *Flight Mechanics of High-Performance Aircraft*, Cambridge Univ. Press, New York, 1993.

[4] Rutowski, E. S., "Energy Approach to the General Aircraft Performance Problem," *Journal of the Aeronautical Sciences*, Vol. 21, No. 3, Mar. 1954, pp. 187–195.

[5] Bryson, A. E., Jr., Desai, M. N., and Hoffman, W. C., "Energy-State Approximation in Performance Optimization of Supersonic Aircraft," *Journal of Aircraft*, Vol. 6, No. 6, Nov.–Dec. 1969, pp. 481–488.

[6] Hill, P. G., and Peterson, C. R., *Mechanics and Thermodynamics of Propulsion*, 2nd ed., Addison–Wesley, New York, 1992.

[7] Nicolai, L. M., *Fundamentals of Aircraft Design*, L. M. Nicolai, Dayton, OH, 1975.

[8] Bryson, A. E., and Ho, Y-C., *Applied Optimal Control*, Blaisdell, Waltham, MA, 1969, p. 17.

[9] Mattingly, J. D., Heiser, W. H., and Daley, D. H., *Aircraft Engine Design*, AIAA Education Series, AIAA, New York, 1987.

[10] Taylor, J. W. R. ed., *Jane's All the World's Aircraft 1983-84*, Jane's Publishing, Inc., New York, 1983, pp. 446–448.